Solid State Ionics 274 (2015) 29–33

Contents lists available at ScienceDirect

Solid State Ionics

journal homepage: www.elsevier.com/locate/ssi

First principles hybrid DFT calculations of $BaTiO_3/SrTiO_3(001)$ interface

Sergei Piskunov, Roberts I. Eglitis *

Institute of Solid State Physics, University of Latvia, 8 Kengaraga Str., Riga LV-1063, Latvia

ARTICLE INFO

Article history:
Received 3 November 2014
Received in revised form 18 February 2015
Accepted 23 February 2015
Available online xxxx

Keywords:
$BaTiO_3/SrTiO_3(001)$ interface
Hybrid DFT calculations
Optical band gap
Ti–O bond covalency

ABSTRACT

We present a first-principles study of $BaTiO_3/SrTiO_3(001)$ interfaces taking into account non-stoichiometric compositions. By means of hybrid exchange–correlation functional within density functional theory (DFT) we demonstrate that charge redistribution in the interface region weakly affects the electronic structure of studied material, while change in the stoichiometry (termination of deposited $BaTiO_3(001)$ thin film) yields in significant shifts of band edges. The optical band gap of $BaTiO_3/SrTiO_3(001)$ interface depends mostly on BaO or TiO_2 termination of the upper layer. Based on results of our calculations we predict enhancement of the Ti–O chemical bond covalency near the $BaTiO_3/SrTiO_3(001)$ interface as compared to the $BaTiO_3$ bulk.

1. Introduction

Recently emerging technologies allow the growth of superlattices and ultrathin films with atomic control. The development of oxide interfaces is a very promising field due to potential nanoscale device applications. Despite the huge technological importance of $SrTiO_3$ (STO) and $BaTiO_3$ (BTO) perovskites, and numerous ab initio studies of their (001) surfaces [1–14], it is hard to understand why only a few ab initio and experimental studies exist dealing with BTO/STO(001) interfaces [15,16].

In this contribution, we intend to present an overview of charge density redistribution in both stoichiometric and non-stoichiometric atomically sharp interfaces consisting of BTO(001) thin film, having a thickness from 1 to 10 monolayers (0.5–5.0 unit cells) deposited atop of TiO_2-terminated STO(001) substrate. The first principle methods we use for simulations are based on density functional theory (DFT) accompanied by hybrid exchange–correlation functional. The B3PW functional [17] used in the current study contains a "hybrid" of the DFT exchange and correlation functionals with exact non-local Hartree–Fock (HF) exchange. Classical BTO and STO low index surfaces have already been thoroughly studied by us previously [1,2,7,8,13].

The paper is structured as follows. Section 2 describes the computational details of our calculations. The main part of the paper is formed by Sec. 3, which presents electronic charge distribution and changes in band structure for BTO/STO interfaces and discusses their relation to the experimental and computational data available in the literature. Our conclusions are summarized in Section 4.

2. Details of numerical simulations

In this study BTO/STO(001) interfaces are simulated by means of linear combination of atomic orbitals (LCAO) within the framework of a hybrid density functional approach. In order to perform hybrid LCAO calculations, we used the periodic crystal code [18], which employs Gaussian-type functions centered on atomic nuclei as the basis sets (BSs). In our study we used the following BSs: For Ba, Sr, Ti and O in the form of 311d1G, 411d311dG, and 8-411d1G, respectively, from Ref. [19]. The inner core electrons of Ba, Sr and Ti are described by small-core Hay–Wadt effective pseudopotentials [20].

We use the well-known hybrid B3PW exchange–correlation functional [17] which accurately describes the basic bulk and surface properties of a number of ABO_3 materials [19,21,22]. The band gaps obtained by means of the hybrid B3PW computation scheme are in better agreement with experimentally observed results than pure DFT calculations [19]. Bond populations and effective charges on atoms have been calculated according to the Mulliken population analysis [23–26]. In our calculations the reciprocal space integration was performed by sampling the Brillouin zone with the $8 \times 8 \times 1$ Pack–Monkhorst mesh [27] for all interface structures under consideration.

Taking into account that the STO substrate at room temperature possesses perfect cubic structure, in our study we calculate both BTO and STO in their high symmetry cubic $Pm\bar{3}m$ phase. Table 1 contains bulk properties simulated for both perovskites. Surface structures were modeled using a single slab model. To maximize the use of symmetry our slabs are symmetrically terminated. STO(001) substrate contains 11 alternating (SrO) and (TiO_2) atomic monolayers, while from 1 to 10 alternating (BaO) and (TiO_2) atomic monolayers were

* Corresponding author. Mobile: +371 26426703.
E-mail addresses: piskunov@lu.lv (S. Piskunov), rieglitis@gmail.com (R.I. Eglitis).

http://dx.doi.org/10.1016/j.ssi.2015.02.020
0167-2738/

Table 1
Equilibrium lattice constants (a_0 in Å), atomic net charges (Q_{atom} in e), cation–O bond populations ($P_{A/B-O}$ in milli e), and band gaps (δ in eV) of bulk BTO and STO in their high-symmetry $Pm\bar{3}m$ cubic phase are calculated by means of B3PW hybrid exchange–correlation functional within DFT. Negative bond population means atomic repulsion. Available experimental data are listed for comparison. Indirect experimentally observed band gaps are listed in this table.

	BTO (B3PW)	BTO (Exp.)	STO (B3PW)	STO (Exp)
a_0	4.007	4.00 [28]	3.903	3.905 [29]
$Q_{Ba/Sr}$	1.79	–	1.87	–
Q_{Ti}	2.36	–	2.35	–
Q_O	−1.39	–	−1.41	–
$P_{Ba/Sr-O}$	−.34	–	−10	–
P_{Ti-O}	100	–	88	–
P_{O-O}	−36	–	−44	–
δ	3.50	3.2 [30]	3.63	3.25 [31]

used for BTO(001) film of the BTO/STO(001) interface (Fig. 1). Coordinates of all atoms in the BTO/STO(001) interfaces were allowed to relax. Due to symmetry constraints atomic displacements are allowed only along the z-axis. Taking into account that the mismatch of ~2.5% between BTO and STO lattice constants arises during BTO epitaxial growth, in our simulations we have allowed relaxation of their joint lattice constant to minimize the strain effect. The equilibrium joint average lattice constant used in the calculations is equal to 3.958 Å. This lattice parameter was calculated for the thickest interface consisting of 10 BTO atomic monolayers deposited at STO substrate and is further used as a reference. Computing Δz displacement for each monolayer of BTO/STO(001) interface we took into account the displacement of the preceding atomic monolayer. The reference z-coordinate for each monolayer N is defined as follows:

$$z_N^{ref} = \frac{1}{2}\left(z_{N-1}^{Me} + z_{N-1}^{O}\right), \quad (1)$$

where z_{N-1}^{Me} and z_{N-1}^{O} are the z-coordinates of the cation and the anion of a preceding atomic monolayer, respectively.

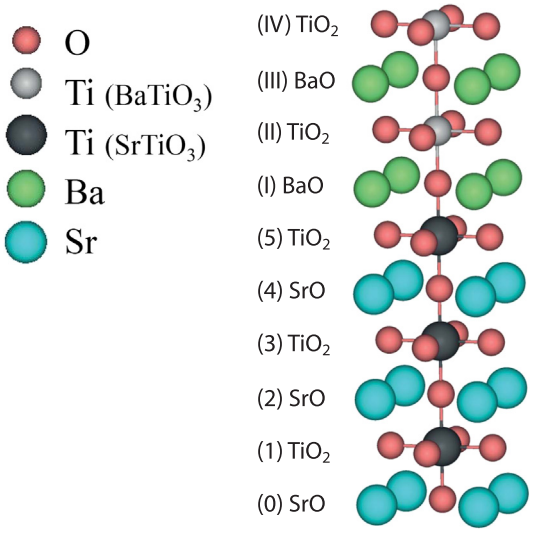

Fig. 1. (Color online) Schematic view of the (001) interface between the two band insulators BTO and STO. Planes of STO(001) substrate are numbered with Arabic numbers, while Roman numbers are used to number planes of deposited BTO(001) film. Zero corresponds to the central plane on symmetrically terminated slab.

3. Results and discussion

Simulations of atomic and electronic properties of the BTO/STO(001) interfaces were performed using the symmetrically terminated slab model. The STO(001) substrate consisted of 11 atomic monolayers and is terminated with a (TiO_2) monolayer. Then monolayer-by-monolayer epitaxial growth was modeled adding a pair of respective monolayers of BTO(001) symmetrically to both sides of a substrate slab until the deposited BTO(001) thin film reaches a thickness of up to 10 monolayers (Fig. 1). In such a way we construct 10 heterostructures consisting of different thickness of deposited BTO nanofilm. Due to the restrictions imposed by the symmetry, in our simulations atomic positions of all atoms were relaxed along the z-axis only. Displacements Δz were calculated with respect to the averaged position z of the previous atomic monolayer as defined in Eq. (1) to avoid constant increase in the value of the former. The obtained results are summarized in Table 2. From Table 2 one can see that all the displacements are within 5% of the lattice constant. The STO(001) substrate expands on the average with respect to the bulk phase, while the BTO(001) thin film, on the contrary, contracts to compensate the lattice mismatch.

In Table 2 we list the net charges of TiO_2, SrO, and BaO atomic planes, as well as in-plane net charges, as calculated for the BTO/STO(001) interfaces under study. Due to the partly covalent nature of Ti–O bonds net charges of Ti, and O deviate from their formal ionic values of +4, and −2, respectively. Mulliken net charges calculated for STO and BTO in their bulk phase are listed in Table 1. As we have shown in our recent studies the Ti–O bond near the BTO and STO (001) surface increases its covalency. Similarly, an increase of the Ti–O chemical bond covalency as compared to the BTO bulk (126 vs. 100 milli e), is observed also near the BTO/STO(001) interface. According to Table 2 the surface atomic planes of TiO_2-terminated BTO(001) films deposited atop STO(001) substrate attract ~0.25 electrons, while BaO-terminated BTO/STO(001) interfaces become more positive to compensate surface relaxation. Thus, the covalency of the surface Ba–O bond is only slightly increased, while the calculated covalency of surface Ti–O bond is larger than in the bulk, which to some extent, may compensate relatively modest surface relaxation of BaO-terminated BTO/STO(001) interfaces with respect to the TiO_2-terminated ones. In both stoichiometric, TiO_2-terminated, and non-stoichiometric, BaO-terminated interfaces, charges on the substrate monolayers did not vary substantially. For stoichiometric and non-stoichiometric interfaces these are about $\pm 0.03e$ for TiO_2 and BaO, respectively. The most significant deviations in atomic charges of BTO/STO(001) structures are located in the top-most monolayer – $\pm 0.26e$ for stoichiometric structures and $-0.23e$ for non-stoichiometric ones – due to the surface effects.

An additional possibility to analyze the electronic charge density redistribution is to recognize what occurs in the electronic charge density in the heterostructures, compared to the isolated BTO(001) and STO(001) slab constituents. Charge density redistribution is defined as the electronic density in the heterointerface minus the sum of electron densities in separately isolated STO(001) substrate and BTO(001) thin film slabs and is depicted in Fig. 2 for both 3- and 4-UC thick BTO/STO(001) interfaces. These plots show us that the most significant distortions occur at the interface due to the compensation of the surface effects of the slabs. They also show that the electronic structure of the substrate of non-stoichiometric heterostructures is distorted similarly to that of stoichiometric ones. The situation in the thin films is opposite. This fact correlates with the argument in the part on atomic structure.

Figs. 2 and 3 show the density of states (DOS) projected layer by layer onto all orbitals of Ba, Sr, Ti, and O atoms of 3- and 4-UC thick BTO/STO(001) interfaces. As in the case of bulk perovskites the top of the valence band is formed by O 2p orbitals, while the bottom of the conduction band is formed mainly by Ti 3d states. Ti–O hybridization is well pronounced. The calculated band gaps of 3.63 eV for STO

Table 2
Calculated atomic net charges (Q_{atom} in e), in-plane net charges (Q_{plane} in e), relative in-plane displacement (Δz in percent of lattice constant) with respect to the perfect bulk positions of perovskite metal atoms, and band gaps (δ in eV) of BTO/STO(001) interfaces under study. Planes of STO(001) substrate numbered with Arabic numbers, while Roman numbers are used to number planes of deposited BTO(001) film. Zero corresponds to the central plane on symmetrically terminated slab.

Layer		STO	BTO-1	BTO-2	BTO-3	BTO-4	BTO-5	BTO-6	BTO-7	BTO-8	BTO-9	BTO-10
X	Q_{Ti}											2.30
	Q_O											−1.27
	Q_{plane}											−0.23
	Δz											−3.92
XI	Q_{Ba}										1.75	1.76
	Q_O										−1.48	−1.37
	Q_{plane}										0.27	0.39
	Δz										−2.32	4.60
VIII	Q_{Ti}									2.30	2.37	2.36
	Q_O									−1.26	−1.41	−1.36
	Q_{plane}									−0.23	−0.44	−0.36
	Δz									−3.84	3.65	0.65
VII	Q_{Ba}								1.75	1.76	1.80	1.79
	Q_O								−1.48	−1.37	−1.42	−1.40
	Q_{plane}								0.26	0.39	0.38	0.39
	Δz								−2.21	4.62	0.68	2.12
VI	Q_{Ti}							2.30	2.37	2.36	2.36	2.36
	Q_O							−1.26	−1.40	−1.36	−1.38	−1.37
	Q_{plane}							−0.23	−0.43	−0.36	−0.40	−0.38
	Δz							−3.70	3.69	0.74	1.88	1.50
V	Q_{Ba}						1.75	1.76	1.80	1.79	1.79	1.79
	Q_O						−1.49	−1.38	−1.42	−1.40	−1.41	−1.41
	Q_{plane}						0.26	0.38	0.37	0.39	0.39	0.39
	Δz						−2.07	4.68	0.76	2.15	1.40	1.71
IV	Q_{Ti}					2.30	2.37	2.36	2.36	2.36	2.36	2.36
	Q_O					−1.26	−1.40	−1.36	−1.38	−1.37	−1.38	−1.37
	Q_{plane}					−0.22	−0.43	−0.36	−0.40	−0.38	−0.39	−0.39
	Δz					−3.55	3.73	0.83	1.92	1.57	1.57	1.63
III	Q_{Ba}				1.75	1.76	1.80	1.79	1.79	1.79	1.79	1.79
	Q_O				−1.49	−1.39	−1.43	−1.41	−1.41	−1.41	−1.40	−1.41
	Q_{plane}				0.25	0.38	0.37	0.38	0.39	0.38	0.39	0.38
	Δz				−1.84	4.77	0.89	2.27	1.48	1.79	1.53	1.68
II	Q_{Ti}			2.29	2.37	2.35	2.36	2.36	2.36	2.36	2.36	2.36
	Q_O			−1.25	−1.40	−1.35	−1.38	−1.37	−1.38	−1.37	−1.38	−1.37
	Q_{plane}			−0.21	−0.42	−0.35	−0.39	−0.37	−0.39	−0.38	−0.39	−0.39
	Δz			−3.20	3.83	1.03	2.04	1.72	1.69	1.75	1.60	1.71
I	Q_{Ba}		1.75	1.76	1.80	1.79	1.79	1.79	1.79	1.79	1.79	1.79
	Q_O		−1.51	−1.40	−1.44	−1.43	−1.42	−1.42	−1.42	−1.42	−1.41	−1.42
	Q_{plane}		0.23	0.36	0.35	0.36	0.37	0.37	0.38	0.37	0.38	0.37
	Δz		−1.54	4.87	1.02	2.35	1.53	1.84	1.55	1.70	1.51	1.64
5	Q_{Ti}	2.29	2.37	2.35	2.36	2.36	2.36	2.36	2.36	2.36	2.36	2.36
	Q_O	−1.29	−1.41	−1.38	−1.40	−1.39	−1.40	−1.40	−1.40	−1.40	−1.40	−1.40
	Q_{plane}	−0.30	−0.45	−0.40	−0.44	−0.42	−0.44	−0.43	−0.44	−0.44	−0.45	−0.44
	Δz	−5.95	1.96	−1.13	−0.11	−0.46	−0.47	−0.43	−0.56	−0.48	−0.61	−0.53
4	Q_{Sr}	1.85	1.88	1.87	1.87	1.87	1.87	1.87	1.87	1.87	1.87	1.87
	Q_O	−1.37	−1.41	−1.39	−1.38	−1.38	−1.37	−1.38	−1.37	−1.37	−1.36	−1.37
	Q_{plane}	0.48	0.47	0.48	0.50	0.49	0.50	0.50	0.51	0.50	0.51	0.50
	Δz	4.13	−1.32	0.60	−0.43	−0.10	−0.39	−0.26	−0.43	−0.33	−0.47	−0.37
3	Q_{Ti}	2.35	2.36	2.36	2.36	2.36	2.36	2.36	2.36	2.36	2.36	2.36
	Q_O	−1.38	−1.42	−1.41	−1.42	−1.41	−1.42	−1.42	−1.43	−1.42	−1.43	−1.42
	Q_{plane}	−0.42	−0.48	−0.45	−0.48	−0.47	−0.49	−0.48	−0.49	−0.48	−0.49	−0.49
	Δz	−0.96	0.27	−0.20	−0.25	−0.21	−0.38	−0.29	−0.44	−0.35	−0.48	−0.40
2	Q_{Sr}	1.87	1.87	1.87	1.87	1.87	1.87	1.87	1.87	1.87	1.87	1.87
	Q_O	−1.42	−1.40	−1.41	−1.39	−1.40	−1.39	−1.39	−1.38	−1.39	−1.38	−1.39
	Q_{plane}	0.45	0.47	0.46	0.48	0.47	0.49	0.48	0.49	0.48	0.49	0.49
	Δz	0.88	−0.35	0.12	−0.29	−0.15	−0.37	−0.26	−0.42	−0.32	−0.45	−0.37
1	Q_{Ti}	2.35	2.36	2.36	2.36	2.36	2.36	2.36	2.36	2.36	2.36	2.36
	Q_O	−1.40	−1.42	−1.41	−1.42	−1.42	−1.42	−1.42	−1.43	−1.42	−1.43	−1.42
	Q_{plane}	−0.44	−0.47	−0.46	−0.48	−0.47	−0.49	−0.48	−0.49	−0.48	−0.49	−0.49
	Δz	0.14	−0.09	−0.01	−0.27	−0.17	−0.36	−0.26	−0.42	−0.33	−0.46	−0.37
0	Q_{Sr}	1.87	1.87	1.87	1.87	1.87	1.87	1.87	1.87	1.87	1.87	1.87
	Q_O	−1.42	−1.40	−1.41	−1.39	−1.40	−1.39	−1.39	−1.38	−1.39	−1.38	−1.39
	Q_{plane}	0.45	0.47	0.46	0.48	0.47	0.49	0.48	0.49	0.48	0.49	0.49
	Δz	0.00	0.00	0.00	0.00	0.00	0.00	0.00	0.00	0.00	0.00	0.00
	δ	2.58	3.47	2.33	3.29	2.16	3.25	2.10	3.24	2.06	3.22	2.06

and 3.50 eV for BTO are in good agreement with experimentally observed indirect gaps of 3.25 and 3.2 eV, respectively [19]. In the case of BaO-terminated BTO/STO(001) interface (Fig. 3) gained excess of electron density shifts the occupied levels up that gives rise to an expanded band gap (Table 2). In turn the TiO_2-terminated interface (Fig. 4) experiences a lack of electron density that shifts the occupied levels down and thus reduces the band gap of stoichiometric BTO/STO(001) interfaces (Fig. 5).

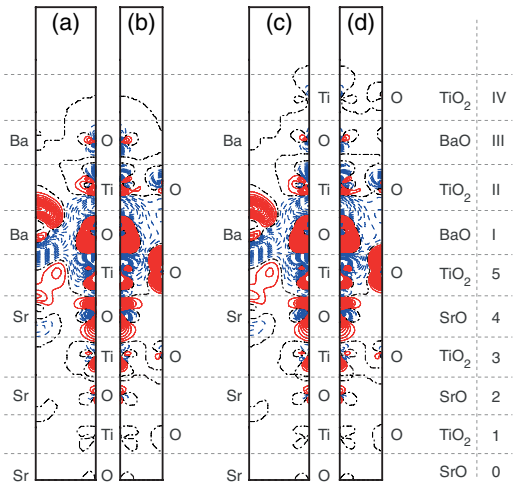

Fig. 2. (Color online) Difference electron charge density maps calculated for BTO/STO(001) heterostructures: (a) (110) cross-section for $N_{BTO} = 3$, (b) (100) cross-section for $N_{BTO} = 3$, (c) (110) cross-section for $N_{BTO} = 4$, (d) (100) cross-section for $N_{BTO} = 4$. Red solid (dark gray), blue dashed (light gray) and black dash-dot isolines describe positive, negative and zero values of the difference charge density, respectively. Isodensity curves are drawn from −0.025 to +0.025 e Å^{-3} with an increment of 0.0005 e Å^{-3}. Right-side bar shows the atomic monolayers from which atoms are originated. Calculations are performed using B3PW hybrid exchange–correlation functional. STO and BTO monolayers are numbered beginning from the center of slab (0 means the central monolayer of the symmetrical slab unit cell). Monolayers (planes) are numbered separately for STO(001) substrate and for BTO(001) nanofilm with Arabic and Roman numbers, respectively.

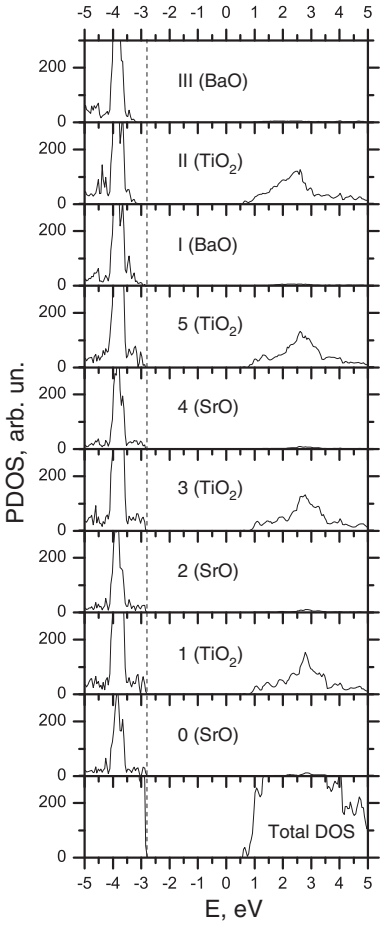

Fig. 3. Layer by layer projected density of states of 3 UC thick BTO/STO(001) interface as calculated by means of B3PW hybrid exchange–correlation functional. Energy scale with respect to vacuum level.

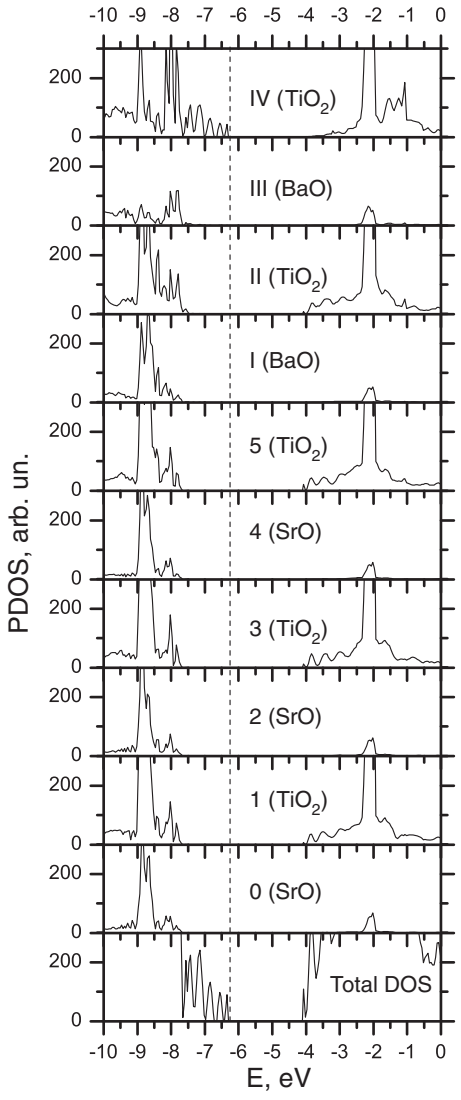

Fig. 4. Layer by layer projected density of states of 4 UC thick BTO/STO(001) interface as calculated by means of B3PW hybrid exchange–correlation functional. Energy scale with respect to vacuum level.

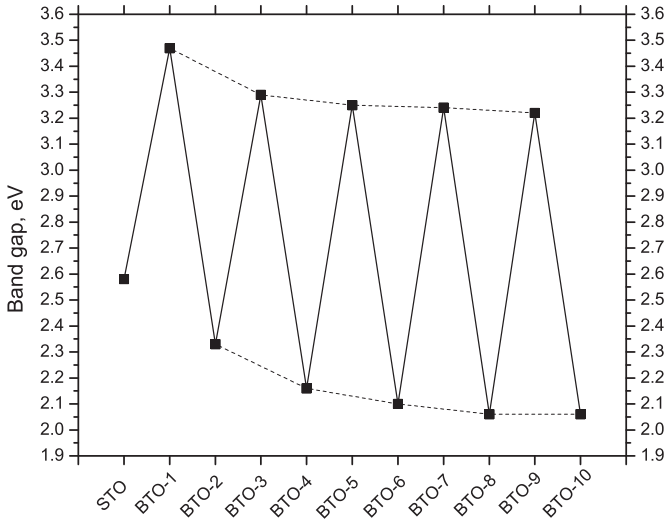

Fig. 5. Calculated optical band gaps of BTO/STO(001) interfaces under study (see Table 2 for details). Number of deposited BTO monolayers changes from zero (TiO_2-terminated STO substrate) to 10. Dashed lines are guide for eyes.

4. Summary and concluding remarks

We have performed ab initio calculations on a number of both stoichiometric and non-stoichiometric BTO/STO(001) heterostructures. For the BTO/STO(001) interface the Ti–O chemical bond population is independent from the number of layers and larger than in the bulk. We find that surface covalent effects in non-stoichiometric films are less pronounced than in stoichiometric ones. All BTO/STO(001) interfaces under study are semiconducting. In agreement with a recent experimental study [16] we found that the interface layer does not influence much the electronic structure of studied structures, while the termination of deposited BTO(001) thin film atop STO (001) substrate may shift the band edges with respect to the vacuum level and thus reduce the band gap. From our point of view such a prediction should be considered for further investigation of BTO/STO(001) heterostructures.

Acknowledgments

This work was supported by the Latvian Council of Science grant No. 374/2012 and ESF grant No. 2013/0046/1DP/1.1.1.2.0/13/APIA/VIAA/021.

References

[1] R.I. Eglitis, D. Vanderbilt, Phys. Rev. B 77 (2008) 195408.
[2] R.I. Eglitis, D. Vanderbilt, Phys. Rev. B 76 (2007) 155439.
[3] A. Höfer, M. Fechner, K. Duncker, M. Hölzer, I. Mertig, W. Widdra, Phys. Rev. Lett. 108 (2012) 087602.
[4] A.M. Kolpak, D. Li, R. Shao, A.M. Rappe, D.A. Bonnell, Phys. Rev. Lett. 101 (2008) 036102.
[5] N. Erdman, K.R. Poeppelmeier, M. Asta, O. Warschkow, D.E. Ellis, L.D. Marks, Nature 419 (2002) 55.
[6] M. Dawber, K.M. Rabe, J.F. Scott, Rev. Mod. Phys. 77 (2005) 1083.
[7] R.I. Eglitis, Int. J. Mod. Phys. B 28 (2014) 1430009.
[8] E. Heifets, R.I. Eglitis, E.A. Kotomin, J. Maier, G. Borstel, Phys. Rev. B 64 (2001) 235417.
[9] J. Dionot, G. Geneste, C. Mathieu, N. Barrett, Phys. Rev. B 90 (2014) 014107.
[10] E. Blokhin, R.A. Evarestov, D. Gryaznov, E.A. Kotomin, J. Maier, Phys. Rev. B 88 (2013) 241407.
[11] Y. Kim, R.M. Lutchyn, C. Nayak, Phys. Rev. B 87 (2013) 245121.
[12] Z. Zhong, A. Tóth, K. Held, Phys. Rev. B 87 (2013) 161102.
[13] R.I. Eglitis, G. Borstel, E. Heifets, S. Piskunov, E.A. Kotomin, J. Electroceram. 16 (2006) 289.
[14] R.A. Evarestov, A.V. Bandura, D.D. Kuruch, J. Comput. Chem. 34 (2013) 175.
[15] V. Stepkova, P. Marton, N. Setter, J. Hlinka, Phys. Rev. B 89 (2014) 060101.
[16] Z. Bi, B.P. Uberuaga, L.J. Vernon, E. Fu, Y. Wang, N. Li, H. Wang, A. Misra, Q.X. Jia, J. Appl. Phys. 113 (2013) 023513.
[17] A.D. Becke, J. Chem. Phys. 98 (1993) 5648.
[18] R. Dovesi, V.R. Saunders, C. Roetti, R. Orlando, C.M. Zicovich-Wilson, F. Pascale, B. Civalleri, K. Doll, N.M. Harrison, I.J. Bush, Ph. D'Arco, M. Llunell, CRYSTAL09 User's Manual, Organization University of Torino, Torino, 2009. (http://www.crystal.unito.it/).
[19] S. Piskunov, E. Heifets, R.I. Eglitis, G. Borstel, Comput. Mater. Sci 29 (2004) 165.
[20] P.J. Hay, W.R. Wadt, J. Chem. Phys. 82 (1984) 299.
[21] S. Piskunov, A. Gopeyenko, E.A. Kotomin, Y.F. Zhukovskii, D.E. Ellis, Comput. Mater. Sci. 41 (2007) 195.
[22] S. Piskunov, E. Spohr, T. Jacob, E.A. Kotomin, D.E. Ellis, Phys. Rev. B 76 (2007) 012410.
[23] R.S. Mulliken, J. Chem. Phys. 23 (1955) 1833.
[24] R.S. Mulliken, J. Chem. Phys. 23 (1955) 184.
[25] R.S. Mulliken, J. Chem. Phys. 23 (1955) 2338.
[26] R.S. Mulliken, J. Chem. Phys. 23 (1955) 2343.
[27] H.J. Monkhorst, J.D. Pack, Phys. Rev. B 13 (1976) 5188.
[28] K.H. Hellwege, A.M. Hellwege (Eds.), Landolt–Bornstein, New Series, vol. 3, Springer Verlag, Berlin, 1969 group III.
[29] Y.A. Abramov, V.G. Tsirelson, V.E. Zavodnik, S.A. Ivanov, I.D. Brown, Acta Crystallogr. B 51 (1995) 942.
[30] S.H. Wemple, Phys. Rev. B 2 (1970) 2679.
[31] K. van Benthem, C. Elsässer, R.H. French, J. Appl. Phys. 90 (2001) 6156.